

# StarryGazer: Leveraging Monocular Depth Estimation Models for Domain-Agnostic Single Depth Image Completion

Sangmin Hong<sup>1†</sup>, Suyoung Lee<sup>2†</sup>, Kyoung Mu Lee<sup>1,2\*</sup>

<sup>1</sup>IPAI, Seoul National University, Seoul 08826, South Korea.

<sup>2</sup>Department of Electrical and Computer Engineering, ASRI, Seoul National University, Seoul 08826, South Korea.

\*Corresponding author(s). E-mail(s): [kyoungmu@snu.ac.kr](mailto:kyoungmu@snu.ac.kr);

Contributing authors: [mchiash2@snu.ac.kr](mailto:mchiash2@snu.ac.kr); [esw0116@snu.ac.kr](mailto:esw0116@snu.ac.kr);

†These authors contributed equally to this work.

## Abstract

The problem of depth completion involves predicting a dense depth image from a single sparse depth map and an RGB image. Unsupervised depth completion methods have been proposed for various datasets where ground truth depth data is unavailable and supervised methods cannot be applied. However, these models require auxiliary data to estimate depth values, which is far from real scenarios. Monocular depth estimation (MDE) models can produce a plausible relative depth map from a single image, but there is no work to properly combine the sparse depth map with MDE for depth completion; a simple affine transformation to the depth map will yield a high error since MDE are inaccurate at estimating depth difference between objects. We introduce **StarryGazer**, a domain-agnostic framework that predicts dense depth images from a single sparse depth image and an RGB image without relying on ground-truth depth by leveraging the power of large MDE models. First, we employ a pre-trained MDE model to produce relative depth images. These images are segmented and randomly rescaled to form synthetic pairs for dense pseudo-ground truth and corresponding sparse depths. A refinement network is trained with the synthetic pairs, incorporating the relative depth maps and RGB images to improve the model’s accuracy and robustness. StarryGazer shows superior results over existing unsupervised methods and transformed MDE results on various datasets, demonstrating that our framework exploits the power of MDE models while appropriately fixing errors using sparse depth information.

**Keywords:** Depth completion, Monocular depth estimation, Self-supervised learning, Synthetic dataset.

## 1 Introduction

Navigating through an environment with incomplete sensory information can be likened to finding one’s way in a dense fog with just a flashlight; While a general sense of the surroundings is possible, obtaining a complete visual picture remains

elusive. Similarly, depth data captured by sensors like LiDAR or Time-of-Flight cameras often appear sparse, limited by factors such as sensor range, occlusions, material reflectivity, and environmental conditions. At this juncture, the task of single-image depth completion emerges as a critical challenge. The objective is to reconstruct a comprehensive depth image from sparse depth

data and RGB images, which presents numerous technical challenges.

Depth completion techniques that utilize a single sparse depth and an RGB image to estimate a dense depth image have recently shown significant advancements. These methods [1–11], rooted in supervised learning paradigms, typically require ground-truth annotations to function effectively. Although potent in controlled environments, these supervised approaches encounter challenges when faced with real-world scenarios’ natural variability and unpredictability, where accurate ground-truth data are often scarce or unavailable. Simply using parameters learned from other training datasets will cause severe performance degradation due to the distribution discrepancy between the two datasets.

To overcome the challenges posed by the domain gap and the lack of ground-truth data, several unsupervised depth completion methods have been developed [12–14]. These methods typically optimize the depth estimation by minimizing reprojection errors derived from multi-view images. Although these approaches address some of the limitations that supervised methods face, they heavily depend on auxiliary inputs such as stereo images or monocular video sequences.

Meanwhile, a monocular depth estimation (MDE) model seeks to infer relative depth from a single RGB image. Recent works in MDE [15–19] have significantly improved zero-shot depth estimation using a large number of parameters and large-scale datasets. These methodologies proficiently generate plausible relative depth maps from any given single RGB image, showcasing the potential of deep learning to interpret complex visual contexts. However, as some works [20–22] have pointed out, MDE often fails to measure the depth difference between two objects accurately and faces challenges when determining whether the surface is concave, convex, or planar.

To this end, we introduce **StarryGazer**, a novel framework that effectively exploits and enhances the domain-agnostic capabilities of MDE models. Operating independently of ground-truth depth data, this framework is specifically designed to adapt to the diverse conditions typical of real-world environments, providing a robust solution for depth completion tasks without the constraints of dense depth data. From the observation that the MDE models show prominent depth estimation

accuracy within each object, we segment the depth map with a pre-trained large segmentation model and rescale the depth values of each segment independently to generate synthetic ground-truth. Then, the synthetic sparse depth map is generated by randomly sampling the points from the synthetic depth map. Then, the refinement network is trained to estimate the synthetic GT from the sparse depth map, MDE map, and RGB image. The parameters for rescaling each segment change for every iteration to widen the manifold of the synthetic depth maps and enable accurate metric depth estimation from the given sparse depth and image during inference.

To validate the superiority of our model, we apply an affine transformation to the MDE [18] depth map to match the statistics of the MDE depth map to the given sparse depth map and evaluate the scale-invariant accuracy (SILog [23]) in Table 1. The global transformed depth map, where all values are multiplied and added by a uniform scalar and bias, shows high SILog. The SILog becomes much lower when the affine transforms are applied to each segment independently. This validates the observation that more errors are produced from the relative positions of the objects than from inside each object. However, as shown in Figure 1, segment-wise transformed results include erroneous regions where the area of the segment is too small to get sufficient information from the sparse depth. StarryGazer shows the best SILog and qualitative depth maps. Extensive experiments validate its strong practical applicability, demonstrating competitive performance on real-world datasets and surpassing large-scale pretrained monocular depth estimation models on out-of-domain datasets [24, 25]. Our main contributions can be summarized as follows:

- We introduce StarryGazer, a domain-agnostic single-depth image completion method that does not require ground-truth depth data by exploiting the power of large monocular depth estimation models.
- We devise a novel technique for generating synthetic ground-truth from segmented and rescaled relative depth maps, facilitating the training of our refinement network using only RGB and sparse depth inputs.
- Our method achieves overwhelming performance in various datasets compared to existing

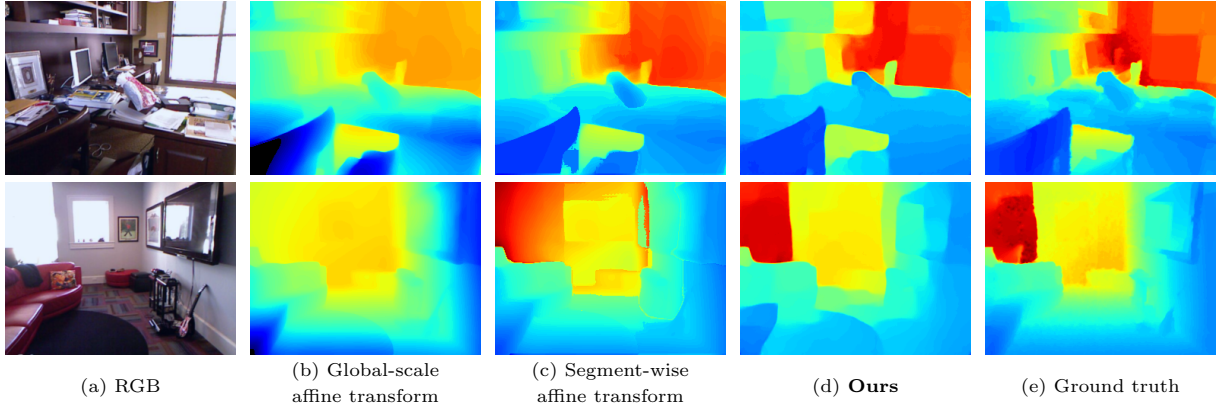


**Fig. 1:** Qualitative comparison of the depth map with the affine-transformed results of depth maps estimated by monocular depth estimators.

**Table 1:** Comparison of scale invariant metric (SILog). The values are multiplied by 100.

Method	SILog $\downarrow$
DepthAnything with global affine transformation	184.87
DepthAnything with segment-wise affine transformation	1.754
<b>Ours</b>	<b>0.022</b>

unsupervised depth completion methods and a simple transformation of monocular depth estimation models.

## 2 Related Works

### Deep monocular depth estimation.

Monocular depth estimation (MDE) has transitioned from its inception using ground-truth-dependent supervised methods, such as convolutional neural networks (CNNs) with scale-invariant loss [26], to sophisticated architectures incorporating conditional random fields [27, 28], regression forests [29, 30], transformer-based encoders [15, 31], and diffusion model [32]. The shift toward self-supervision aims to reduce annotation reliance, leveraging strategies like photometric consistency [33] and mixed reconstruction losses [34]. Recent advances focus on zero-shot depth estimation capable of handling images in varied domains without specific training [15, 16, 19, 35–37], although these methods often struggle with generalization when predicting absolute depths. Our approach combines a domain-agnostic relative depth estimator with a robust absolute

depth model to improve accuracy and generalizability in depth image estimation.

### *Supervised learning for depth completion.*

Depth image completion, the process of estimating dense depth images from sparse data, is crucial for applications such as autonomous navigation. The introduction of image-guided techniques marked a significant advancement, using additional modalities such as RGB images [2, 7], semantic images [38, 39], and surface normals [5] to enrich and refine depth estimation. Recent innovations have evolved to include multi-branch networks [40–45] and spatial propagation networks [1, 3, 4, 46, 47], which integrate these multi-modal inputs through advanced fusion techniques, enhancing the accuracy and structural integrity of the resulting depth images. Despite rapid evolution in the field, these supervised methods still suffer from performance degradation when applied outside their training domain, reflecting an ongoing challenge of domain-agnostic depth completion.

### Unsupervised learning for depth completion.

Unsupervised depth completion methods have emerged as a response to the limitations observed in supervised methods, particularly their performance degradation when applied outside their training domain. These methods [12–14, 43, 44, 48–53] eliminate the need for ground-truth supervision during training. Instead, they used stereo images or monocular videos to compute photometric reprojection errors, minimizing discrepancies between input images and their reconstructions from other perspectives [12, 13, 44, 51–53]. In particular, Wong *et al.* [53] address occlusions by applying adaptive optimization to reduce penalties in these regions, while KBNet [50] introduces a calibrated back projection network that enhances depth estimation accuracy by projecting image pixels onto 3D scenes. Despite their efficacy in handling real-world data, these methods still rely on auxiliary inputs, such as stereo images or monocular video sequences, to function effectively. In contrast, our approach aims to advance depth completion without ground-truth data or additional visual input, thereby overcoming the limitations of current unsupervised methods.

## 3 Method

Our method, StarryGazer, leverages the large generalizable capacity from a pre-trained monocular depth estimation network to estimate depth from RGB images, circumventing the need for ground-truth depth images during training. As illustrated in Figure 2, we first estimate a relative depth map from an off-the-shelf deep monocular depth estimation network and then segment the map into several classes. Then, a synthetic ground-truth depth is generated by adaptively rescaling the values of the depth map in a segment-wise manner. We sample the point from the synthetic ground truth to produce the corresponding synthetic sparse image. The refinement network is trained using the synthetic pairs. This framework introduces realistic depth variability, preparing the refinement model to perform robustly across diverse real-world scenes.

### 3.1 Monocular Depth Estimation

The relative depth images are generated using an existing deep monocular depth estimation network. The process is defined as follows:

$$D_{\text{rel}} = f_{\text{MDE}}(I_{\text{RGB}}), \quad (1)$$

where  $D_{\text{rel}}$  represents the relative depth image produced,  $I_{\text{RGB}}$  denotes the input RGB image and  $f_{\text{MDE}}$  is the monocular depth estimation model. The MDE model captures geometric and semantic cues from a single image by leveraging a large-scale dataset during training.

### 3.2 Generating Synthetic Pairs

A crucial part of our framework is the generation of synthetic pairs to train the refinement network. Although the MDE model tends to estimate the relative depths in the single object accurately, many errors occur at the boundary between the objects where the depth values change rapidly [54]. Therefore, we segment objects in the depth map and then independently rescale the depth values of each segment to add diversity to the depth relationships between objects while maintaining the depth relationships within the objects. Using the off-the-shelf segmentation model, each relative depth image is normalized and segmented to identify distinct regions:

$$M_{\text{seg}} = f_{\text{seg}} \left( \frac{D_{\text{rel}} - \min(D_{\text{rel}})}{\max(D_{\text{rel}}) - \min(D_{\text{rel}})} \right), \quad (2)$$

where  $M_{\text{seg}}$  denotes the segmentation map for the corresponding image and  $f_{\text{seg}}$  is an off-the-shelf semantic segmentation model. The segmentation model discriminates regions based on the normalized depth values. After segmentation, each identified region undergoes a rescaling process. The rescaling is performed adaptively, taking into account the local depth statistics within each region to simulate real-world depth variations more accurately:

$$D_{\text{sg}} = \sum_k (\alpha_k \cdot (D_{\text{rel}} \odot M_{\text{seg}}[k]) + \beta_k), \quad (3)$$

where  $D_{\text{sg}}$  refers to synthetic ground-truth depth and  $\alpha_k$  and  $\beta_k$  are rescaling factors of the relative depth values within the region  $k$ . Here,  $M_{\text{seg}}[k]$

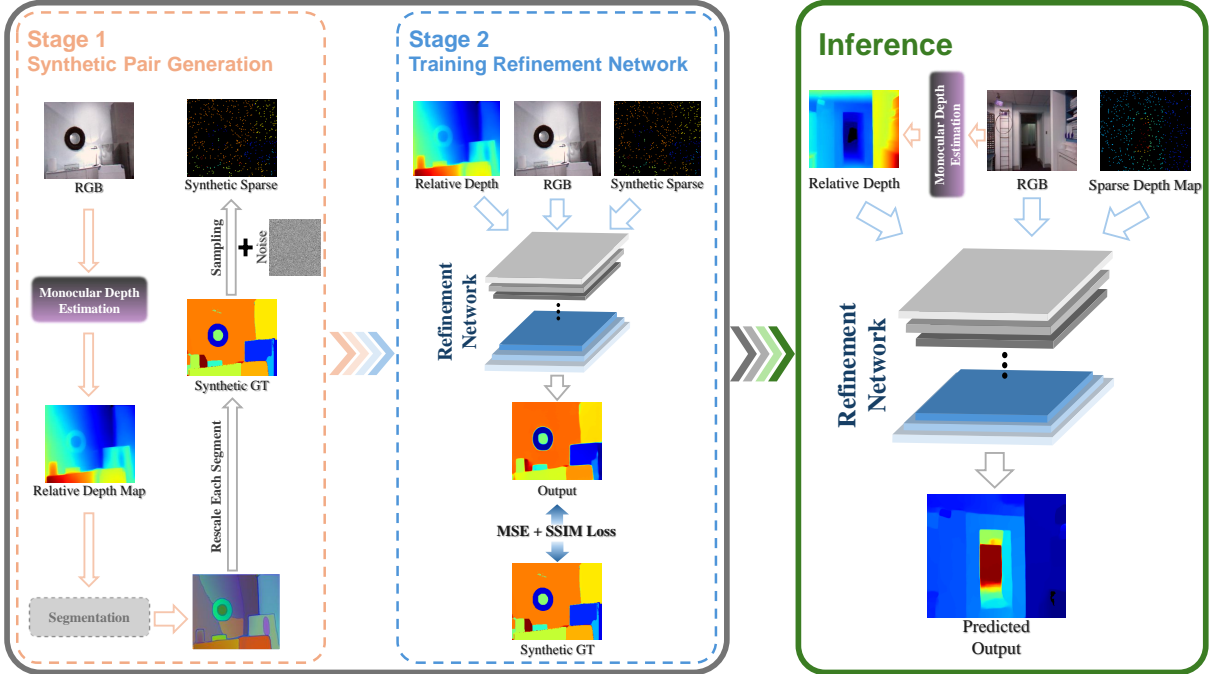


**Fig. 2: Overall Pipeline of StarryGazer.** The training pipeline involves two stages: stage 1 generates synthetic pairs, while stage 2 trains the refinement network using the synthetic pairs. The trained refinement network uses real RGB images and sparse depth inputs to estimate dense depth maps during inference.

denotes the segmentation mask for the  $k$ -th segment, which is set to 1, while all other segments are set to 0. Typically,  $\alpha_k$  is chosen to match the scale of depth variations observed in sparse depth data, while  $\beta_k$  adjusts the baseline depth to align with the observed minima and maxima within the region. The operation  $\odot$  denotes element-wise multiplication, ensuring that the rescaling is applied independently for every segmented region. The adaptive rescaling factors  $\alpha_k$  and  $\beta_k$  are determined as follows:

$$\alpha_k = \frac{2 \cdot \text{mean}(D_s)}{\text{mean}(D_{\text{rel}} \odot M_{\text{seg}}[k])}, \quad (4)$$

$$\beta_k \sim U(\min(D_s), \max(D_s)) - \text{mean}(D_s), \quad (5)$$

where  $U(a, b)$  denotes the uniform distribution over the interval  $[a, b]$  and  $D_s$  is original sparse depth image. These scaling adjustments ensure that the synthetic ground-truth images not only retain the structural integrity of the scene but also increase depth variability to encompass real-world depth distribution. After rescaling, gaps or holes within the synthetic images where depth data

might be missing due to incomplete segmentation masks are filled using an average filter. This process enhances the continuity of the synthetic depth images, which is crucial for training the refinement model. Then, synthetic sparse images are produced by applying the original sparse image as a mask, adding Gaussian noise to complement sensor inaccuracies robustly.

$$D_{ss} = (D_{sg} + \mathcal{N}(0, \sigma^2)) \odot M_s, \quad (6)$$

where  $D_{ss}$ ,  $D_{sg}$  refers to synthetic sparse depth image and synthetic ground-truth depth image, respectively, and  $M_s$  refers to the mask obtained from the original sparse depth map for  $I_{RGB}$ . Adding Gaussian noise preserves the sparsity pattern and introduces realistic variability, enhancing the model performance with real sparse-depth images.

### 3.3 Training Refinement Network

We train the refinement network from the synthetic pairs  $(D_{sg}, D_{ss})$ . The refinement network receives the RGB image ( $I_{RGB}$ ), the synthetic

sparse map ( $D_{ss}$ ) and the relative depth map ( $D_{rel}$ ) and is trained to estimate the corresponding synthetic ground truth ( $D_{sg}$ ). Our training objective combines mean squared error (MSE) and structural similarity index measure (SSIM) loss functions, aiming to maximize the pixel-wise accuracy of the predicted depth images relative to the synthetic ground-truth. The MSE loss function calculates the mean squared difference between predicted and ground-truth depth values, defined as:

$$\mathcal{L}^{\text{mse}}(D_{\text{pred}}, D_{\text{sg}}) = \frac{1}{N} \sum_{i=1}^N (D_{\text{pred}}[i] - D_{\text{sg}}[i])^2, \quad (7)$$

where  $N$  is the number of pixels in the depth image,  $D_{\text{pred}}$  is the depth image predicted by the model, and  $D_{\text{sg}}$  represents the synthetic ground-truth depth image.

Meanwhile, the SSIM loss function is used to improve the perceptual quality of predicted depth images by focusing on structural information, which is crucial to human visual perception. However, several works [55, 56] have shown that SSIM loss is also helpful to improve the accuracy of results as well as perceptual quality. This SSIM loss is defined as:

$$\mathcal{L}^{\text{ssim}}(D_{\text{pred}}, D_{\text{sg}}) = 1 - \frac{1}{M} \sum_{j=1}^M (\text{SSIM map})_j, \quad (8)$$

where  $M$  is the total number of local patches within the image, and *SSIM map* is computed as:

$$\text{SSIM map} = \frac{(2 \cdot \mu_{\text{pred}} \cdot \mu_{\text{sg}} + C_1)(2 \cdot \sigma_{\text{pred}, \text{sg}} + C_2)}{(\mu_{\text{pred}}^2 + \mu_{\text{sg}}^2 + C_1)(\sigma_{\text{pred}}^2 + \sigma_{\text{sg}}^2 + C_2)}, \quad (9)$$

where  $\mu_{\text{pred}}$  and  $\mu_{\text{sg}}$  are the local means, and  $\sigma_{\text{pred}}^2$ ,  $\sigma_{\text{sg}}^2$ , and  $\sigma_{\text{pred}, \text{sg}}$  are the local variances and covariance, computed using an averaging filter with a kernel size of 11.  $C_1$  and  $C_2$  are constants that stabilize the division with weak denominator, defined as  $C_1 = (k_1 L)^2$  and  $C_2 = (k_2 L)^2$ , with  $L$  being the dynamic range of the pixel-values (typically set to 1.0), and  $k_1 = 0.01$ ,  $k_2 = 0.03$ .

The overall loss function used to train our model is a weighted sum of the MSE and SSIM losses:

$$\mathcal{L}^{\text{total}} = \mathcal{L}^{\text{mse}} + \lambda \cdot \mathcal{L}^{\text{ssim}}, \quad (10)$$

where  $\lambda$  is a hyperparameter. This combination of two loss terms yields higher depth estimation accuracy, which will be analyzed in detail in Section 4.4.

## 4 Experiment

### 4.1 Datasets

In this work, we utilize several well-established datasets to evaluate the performance and generalization of our depth completion model.

**NYU Depth V2** [57]. Comprising RGB and depth images extracted from video sequences of 464 indoor scenes, NYU Depth V2 has been a standard in depth completion benchmark. We follow conventional pre-processing from previous work [4, 8] by resizing images from  $640 \times 480$  to  $304 \times 228$  and applying random sampling to create sparse depth images. We train on 50,000 training images and evaluate on 654 images from the official test set.

**KITTI Depth Completion (DC)** [58]. Comprising 86,898 training samples along with 1,000 validation and 1,000 test samples, the KITTI Depth Completion dataset is a widely utilized real-world dataset for depth completion. The ground-truth is obtained from 11 LiDAR scans. Consistent with previous studies [8], we modify the image resolution to  $1216 \times 240$  by cropping the bottom center.

**ClearGrasp** [24]. ClearGrasp is a dataset that offers both synthetic and real-world scenarios focused on transparent objects, a challenging domain for depth sensing technologies. Each segment of the ClearGrasp dataset, which comprises synthetic and real subsets, is further divided into training and novel sets. These novel sets contain classes that have not been encountered during the training phase, making the typical depth estimation model generate erroneous depth maps due to the large domain gap.

### 4.2 Implementation Details

We use the DepthAnything VIT-S model [18] and the Segment-Anything VIT-H model [59] for MDE and segmentation, respectively. We note that the datasets used for training DepthAnything and the datasets used for evaluation in this paper are

entirely distinct, ensuring that no privileged information is involved in the pre-trained weights. For the refinement network, we slightly change the first CNN layer of NLSPN [4], allowing the model to simultaneously receive RGB, sparse depth, and relative depth inputs. We use Adam optimizer [60] with a starting learning rate of 0.0001, adjusted by a step scheduler that reduces the rate by 0.8 for every five epochs. We set the loss weighting coefficient  $\lambda$  to 12 for training on the KITTI DC and 3 for the other datasets. We use MAE, RMSE, iMAE, and iRMSE for evaluation metrics. Experiments are conducted on Quadro RTX 8000 GPUs using PyTorch 1.10.1 [61]. More details are provided in the supplementary material.

### 4.3 Evaluation on Various Datasets

#### *Baseline: applying affine transformations to MDE depth maps.*

Since StarryGazer utilizes a large MDE model to train the refinement network, we include the results of the MDE model as baselines for evaluation. However, the MDE model does not utilize the sparse absolute depth map information, and naively comparing the MDE depth maps with our results cannot be considered fair. Thus, we apply a simple mathematical transformation, an affine transformation, to the MDE depth map to match the statistics of the sparse depth map values. Specifically, the affine transformation is applied in two types: global scale and segment-wise. For the global affine transformation case, a single scaling factor and bias are multiplied and added throughout the entire depth map. The two values are determined to minimize the mean squared distance from absolute sparse depth values using the pseudo-inverse matrix. The segment-wise affine transformation applies the affine transformation independently to each segment estimated by the segmentation model ( $f_{seg}$ ). For the segment that does not include any sparse depth points, we just use the MDE output value since there is no information about the statistics of the segment.

#### 4.3.1 NYU V2 Dataset

This section presents both quantitative and qualitative evaluations of our method on the NYU Depth V2 dataset, a widely recognized indoor dataset for depth completion. To ensure a fair

comparison, we assume that no ground-truth depth is available during training, focusing exclusively on unsupervised methods. Table 2 outlines the performance of StarryGazer compared to existing approaches. The unsupervised methods show inferior quality to our results, highlighting the effectiveness of exploiting the prior knowledge from MDE models. For affine transformed MDE maps, both global and segment-wise transformations show poor results. Global transformation cannot correct the inaccuracy of the depth difference between objects in MDE, and cannot reduce the error effectively. In the case of segment-wise transformation, since the sparse depth value of each segment is small, fitting with only the depth information within each segment can form an incorrect distribution with huge errors. Our refinement network, in contrast, shows the best results by appropriately manipulating the depth map from MDE using the information from the global sparse map and the RGB image. Figure 3 visually compares our method with other unsupervised techniques. Although the MDE model effectively captures semantic details and object shapes, it fails to estimate the relative position among the entities, often predicting near- and far-objects in opposite directions. Our method shows considerable qualitative improvements over these models and produces smoother depth images, approaching the quality of actual ground-truth. These visual assessments highlight the efficacy of our approach in generating realistic depth fields from sparse data, underlining its potential for robust real-world applications.

#### 4.3.2 KITTI DC Dataset

We demonstrate the practical applicability of StarryGazer in real-world outdoor scenarios, particularly under conditions where sparse depth data is unevenly distributed. Unlike other unsupervised methods that rely on auxiliary inputs such as stereo images or camera intrinsic matrices, as mentioned in Section 2, our approach operates without such additional data.

Table 3 compares our method quantitatively with other unsupervised learning approaches on the KITTI DC dataset. Our method demonstrates superior performance in terms of MAE and RMSE, achieving the lowest scores of 242.44 mm and 1061.43 mm, respectively. This indicates an

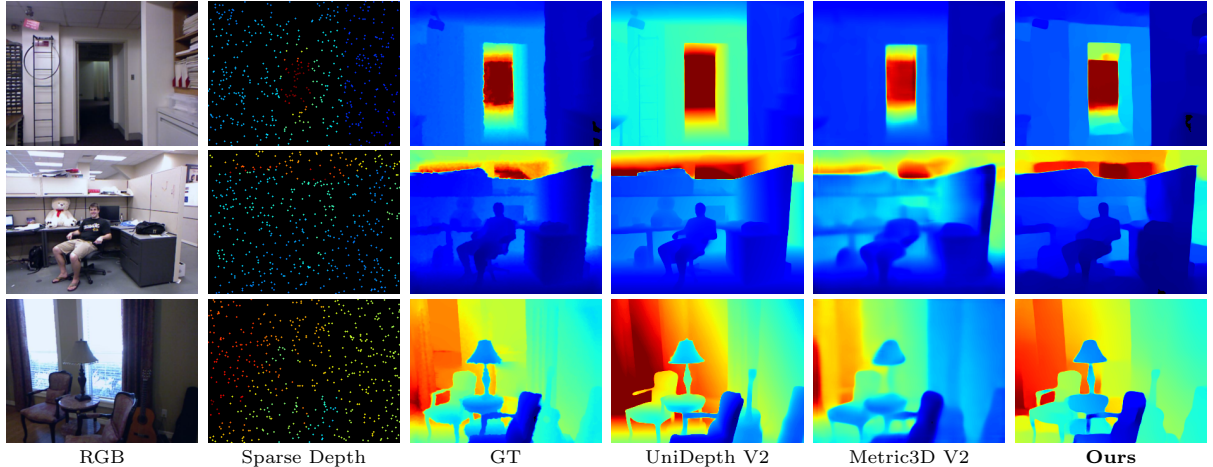


**Fig. 3:** Qualitative comparison on NYU Depth V2 dataset.

**Table 2:** Quantitative results on the NYU Depth V2.

Method		MAE (m)↓	RMSE (m)↓	iMAE (1/km)↓	iRMSE (1/km)↓
Unsupervised	SynthProj [49]	0.134	0.235	29.84	57.13
	VOICED [51]	0.128	0.228	28.89	54.70
	ScaffNet [52]	0.117	0.199	24.89	44.06
	KBNet [50]	0.106	0.198	21.37	42.74
	DesNet [14]	0.103	0.188	21.44	38.57
MDE	DA [18] (Global)	0.334	0.434	193.268	5549.994
	DA [18] (Segment)	0.226	0.514	38.445	164.335
	Metric3D V2 [35] (Global)	1.004	1.037	337.330	368.462
	Metric3D V2 [35] (Segment)	1.031	1.071	345.631	381.167
	UniDepth V2 [36] (Global)	0.828	0.941	115.869	138.387
	UniDepth V2 [36] (Segment)	0.952	1.100	142.706	180.426
Ours		<b>0.100</b>	<b>0.171</b>	<b>18.78</b>	<b>35.93</b>

improvement over competing methods, confirming the effectiveness of our approach in handling diverse driving scenarios. However, in terms of iMAE, our method exhibits a slight underperformance, registering 1.67 compared to the best score of 1.03 by KBNet [50]. This happens because our refinement network is not specially designed for sparsity robustness and produces higher errors at closer ranges, where the errors are more penalized. Meanwhile, our method still shows superiority on iRMSE, which implies that errors in these regions are consistently distributed without significant outliers. Despite this minor limitation, the overall results strongly validate the robustness and reliability of our method in real-world applications. Also, similar to the result in NYU V2, our model outperforms transformed MDE

results with a large margin by exploiting the information from the input image. Figure 4 presents the qualitative comparison on the KITTI DC dataset. The visual results clearly demonstrate that our method not only estimates smoother depth images but also recovers local details more effectively than competing unsupervised methods. These results demonstrate our model’s ability to handle complex outdoor scenes, preserving both major structures and finer details essential for real-world applications.

#### 4.3.3 ClearGrasp Dataset

To demonstrate the generalizability of our model in various domains, we performed evaluations on the ClearGrasp dataset. It has different image

**Table 3:** Quantitative results on the KITTI DC dataset.

Method		MAE (mm)↓	RMSE (mm)↓	iMAE (1/km)↓	iRMSE (1/km)↓
Unsupervised	SS-S2D [12]	350.32	1299.85	1.57	4.07
	DFuseNet [13]	429.93	1206.66	1.79	3.62
	DDP [44]	343.46	1263.19	1.32	3.58
	VOICED [51]	299.41	1169.97	1.20	3.56
	AdaFrame [53]	291.62	1125.67	1.16	3.32
	SynthProj [49]	280.42	1095.26	1.19	3.53
	ScaffNet [52]	280.76	1121.93	1.15	3.30
	KBNet [50]	258.36	1068.07	<b>1.03</b>	3.01
MDE	DA [18] (global)	3877.73	5520.75	147.69	6906.60
	DA [18] (segment)	1794.08	3332.65	15.60	35.54
	Metric3D V2 [35] (global)	3856.70	7903.73	51.67	76.48
	Metric3D V2 [35] (segment)	3257.82	4714.90	38.91	47.48
	UniDepth V2 [36] (global)	6155.49	7783.78	31.92	35.87
	UniDepth V2 [36] (segment)	7060.72	9595.91	36.16	44.95
Ours		<b>242.44</b>	<b>1061.43</b>	1.67	<b>2.81</b>

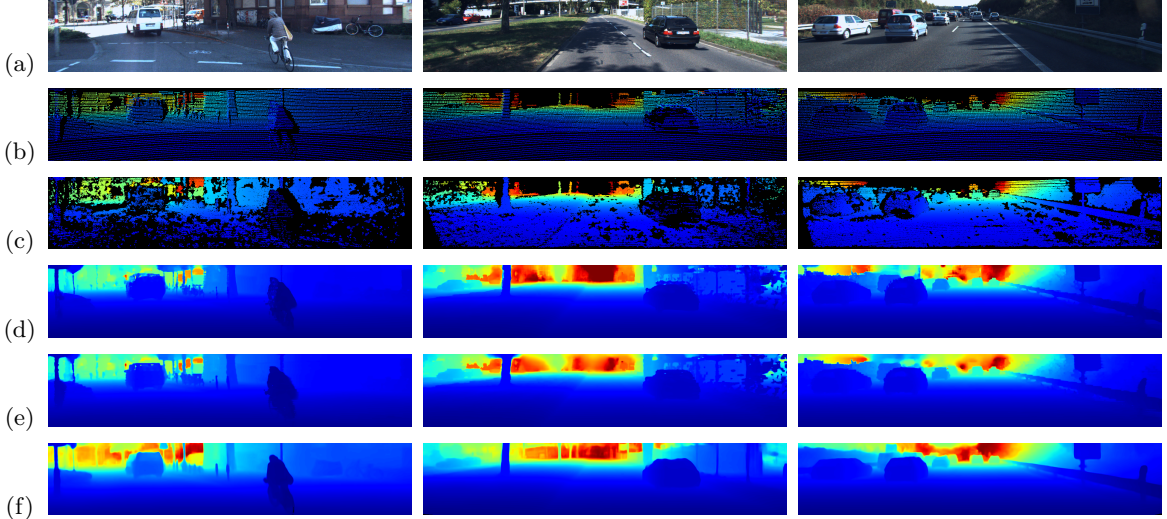


**Fig. 4:** Qualitative comparison on KITTI DC dataset. (a) RGB, (b) Sparse Depth, (c) Ground Truth (d) ScaffNet [52], (e) KBNet [50], (f) Ours.

manifolds from typical datasets used for training supervised depth completion networks. Obtaining ground-truth data is often challenging in real-world scenarios, and maintaining performance in unseen environments is particularly challenging. Our method’s advantage is that it can be trained using synthetically generated pairs without relying on ground-truth data, making it particularly suitable for handling such challenges. Table 4 provides a quantitative comparison of our method against supervised depth completion methods and

transformed MDE methods. Our method achieves the lowest errors on both datasets, underscoring its robustness in out-of-domain scenarios.

As shown in Figure 5, the mask map restricts sparse depth values to non-masked areas, leaving no depth points available for transparent objects. This setup poses a challenge for competing methods that struggle to estimate depth accurately, particularly in regions with transparent objects. In contrast, our method successfully estimates the

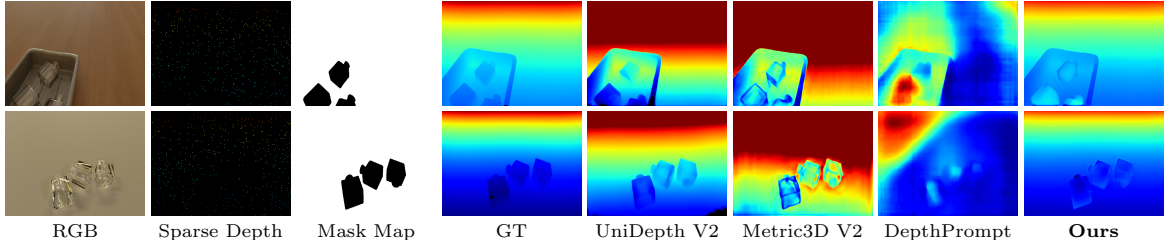


**Fig. 5:** Qualitative comparison on ClearGrasp dataset. In this setting, the mask map restricts sparse depth data to non-masked areas, leaving no depth values for transparent objects.

**Table 4:** Quantitative comparison on ClearGrasp dataset.

	Method	MAE (m)↓	RMSE (m)↓
Supervised	DenseDepth [62]	0.260	0.270
	DeepCompletion [63]	0.045	0.054
	NLSPN [4]	0.106	0.132
	ClearGrasp [24]	0.038	0.044
	LocalImplicit [64]	0.034	0.041
	TranspareNet [65]	0.027	<b>0.032</b>
	Depth Prompting [47]	0.462	0.530
MDE	DA [18](Global)	0.077	0.120
	DA [18](Segment)	0.065	0.139
	Metric3D V2 [35](Global)	0.230	0.261
	Metric3D V2 [35](Segment)	0.221	0.245
	UniDepth V2 [36](Global)	0.296	0.311
	UniDepth V2 [36](Segment)	0.301	0.332
	Ours	<b>0.025</b>	0.062

**Table 5:** Ablations on different values of  $\alpha_k$  and  $\beta_k$ .

$\alpha_k$	$\beta_k$	MAE (m)↓	RMSE (m)↓
Eq. 11	0	2.72	2.91
Eq. 11	Eq. 5	0.234	0.326
Eq. 5	Eq. 5	<b>0.100</b>	<b>0.171</b>

depth values for these objects, producing results that are closely aligned with the ground-truth.

#### 4.4 Ablation Studies

##### *Effect of $\alpha_k, \beta_k$ configuration for training.*

Since the refinement network is trained with synthetic pairs, the synthetic ground-truth should

**Table 6:** Effect of  $\mathcal{L}^{ssim}$  and noise addition.

$\mathcal{L}^{mse}$	$\mathcal{L}^{ssim}$	Noise	MAE (m)↓	RMSE (m)↓
✓	✗	✗	0.132	0.212
✓	✓	✗	0.118	0.190
✓	✗	✓	0.112	0.192
✓	✓	✓	<b>0.100</b>	<b>0.171</b>

be similar to the original depth distribution. We change the configuration of  $\alpha$  and  $\beta$  when generating synthetic ground-truth for training. When we choose  $\alpha$  in a stochastic manner,  $\alpha$  is sampled from the following distribution:

$$\alpha_k \sim U(\min(D_s), \max(D_s)). \quad (11)$$

Table 5 shows the results by changing the distributions of  $\alpha_k$  and  $\beta_k$ . First, giving the fixed value  $\beta_k$  severely degrades the quality. The distribution discrepancy between synthetic GT and real GT remains when we use a fixed  $\beta_k$  value. On the contrary, as  $\beta_k$  varies at each iteration, the distribution of synthetic GTs is expanded to include real GTs. In case of  $\alpha_k$ , making  $\alpha_k$  flexible will over-broaden the distribution of synthetic data, leading the model to be underfitted to such a large distribution. Our configuration shows the best bias-variance tradeoff for designating the distribution of synthetic data.

##### *Effect of $\mathcal{L}^{ssim}$ and noise addition.*

We evaluate the impact on model performance of excluding  $\mathcal{L}^{ssim}$  and adding synthetic noise during training, as shown in Table 6. The omission of  $\mathcal{L}^{ssim}$  from the loss function led to a slight degradation in both MAE and RMSE, highlighting its crucial role in enhancing the smoothness and

visual coherence of the depth images. The absence of noise in the training process also resulted in a modest deterioration in performance, suggesting that the incorporation of noise aids in mimicking the real-world inaccuracies found in sensor data. Removing both  $\mathcal{L}^{ssim}$  and noise led to the most significant performance drop, underlining their combined importance in achieving optimal results. These findings underscore the necessity of both  $\mathcal{L}^{ssim}$  for depth image refinement and synthetic noise for realistic training conditions, affirming their synergistic effect in improving the model's performance in depth completion tasks.

## 5 Conclusion

We introduce StarryGazer, a domain-agnostic approach for depth completion using monocular depth estimation models. The MDE depth maps are segmented and rescaled to generate synthetic sparse and dense depth pairs. The refinement network trained on the synthetic dataset estimates the final dense depth map from the RGB image and the sparse depth map. The training framework leverages the strong prior of depth maps generated by the MDE model while fixing the error of the MDE estimated maps by augmenting the synthetic ground truth using segment-wise rescaling.

**Limitations and future works.** While StarryGazer has shown promising results, the framework will fail where the synthetic ground-truth map cannot imitate the distribution of real depth maps. Future works can involve adaptive segmentation models or an improved rescaling policy that considers the RGB image to generate a more proper synthetic data distribution.

## Statements and Declarations

**Competing interests** The authors declare that they have no known competing financial interests or personal relationships that could have appeared to influence the work reported in this paper. The authors declare the following financial interests/personal relationships which may be considered as potential competing interests.

**Authors contributions** S.H. and S.L. designed the method and conducted the experiments. S.H.

implemented the framework and performed ablation studies. S.L. conducted comparative evaluations. K.M.L. supervised the project and provided critical feedback on the methodology and manuscript.

## References

- [1] Cheng, X., Wang, P., Yang, R.: Depth estimation via affinity learned with convolutional spatial propagation network. In: Proceedings of the European Conference on Computer Vision, pp. 103–119 (2018)
- [2] Hu, M., Wang, S., Li, B., Ning, S., Fan, L., Gong, X.: Towards precise and efficient image guided depth completion (2021)
- [3] Lin, Y., Yang, H., Cheng, T., Zhou, W., Yin, Z.: Dyspn: Learning dynamic affinity for image-guided depth completion. IEEE Transactions on Circuits and Systems for Video Technology, 1–1 (2023) <https://doi.org/10.1109/TCSVT.2023.3321668>
- [4] Park, J., Joo, K., Hu, Z., Liu, C.-K., Kweon, I.S.: Non-local spatial propagation network for depth completion. In: Proceedings of the European Conference on Computer Vision (2020)
- [5] Qiu, J., Cui, Z., Zhang, Y., Zhang, X., Liu, S., Zeng, B., Pollefeys, M.: Deeplidar: Deep surface normal guided depth prediction for outdoor scene from sparse lidar data and single color image. In: Proceedings of the IEEE/CVF Conference on Computer Vision and Pattern Recognition (2019)
- [6] Tang, J., Tian, F.-P., Feng, W., Li, J., Tan, P.: Learning guided convolutional network for depth completion. IEEE Transactions on Image Processing **30**, 1116–1129 (2020)
- [7] Yan, Z., Wang, K., Li, X., Zhang, Z., Li, J., Yang, J.: Rignet: Repetitive image guided network for depth completion. In: Proceedings of the European Conference on Computer Vision, pp. 214–230. Springer, Cham (2022)
- [8] Zhang, Y., Guo, X., Poggi, M., Zhu, Z., Huang, G., Mattoccia, S.: Completionformer: Depth completion with convolutions and vision transformers. In: Proceedings of the IEEE/CVF Conference on Computer Vision and Pattern Recognition, pp. 18527–18536 (2023)

- [9] Imran, S., Liu, X., Morris, D.: Depth completion with twin-surface extrapolation at occlusion boundaries. In: Proceedings of the IEEE/CVF Conference on Computer Vision and Pattern Recognition (2021)
- [10] Conti, A., Poggi, M., Mattoccia, S.: Sparsity agnostic depth completion. In: Proceedings of the IEEE/CVF Winter Conference on Applications of Computer Vision (2023)
- [11] Rho, K., Ha, J., Kim, Y.: Guideformer: Transformers for image guided depth completion. In: Proceedings of the IEEE/CVF Conference on Computer Vision and Pattern Recognition, pp. 6250–6259 (2022)
- [12] Ma, F., Cavalheiro, G.V., Karaman, S.: Self-supervised sparse-to-dense: Self-supervised depth completion from lidar and monocular camera. IEEE International Conference on Robotics and Automation (2019)
- [13] Shivakumar, S.S., Nguyen, T., Miller, I.D., Chen, S.W., Kumar, V., Taylor, C.J.: Dfusenet: Deep fusion of rgb and sparse depth information for image guided dense depth completion. In: IEEE Intelligent Transportation Systems Conference, pp. 13–20 (2019). <https://doi.org/10.1109/ITSC.2019.8917294>
- [14] Yan, Z., Wang, K., Li, X., Zhang, Z., Li, J., Yang, J.: Desnet: Decomposed scale-consistent network for unsupervised depth completion. In: Proceedings of the AAAI Conference on Artificial Intelligence (2023). AAAI
- [15] Bhat, S.F., Birk, R., Wofk, D., Wonka, P., Müller, M.: Zoodepth: Zero-shot transfer by combining relative and metric depth. arXiv preprint arXiv:2302.12288 (2023) [arXiv:2302.12288 \[cs.CV\]](https://arxiv.org/abs/2302.12288)
- [16] Guizilini, V., Vasiljevic, I., Chen, D., Ambrus, R., Gaidon, A.: Towards zero-shot scale-aware monocular depth estimation. In: Proceedings of the IEEE/CVF International Conference on Computer Vision (2023)
- [17] Ranftl, R., Lasinger, K., Hafner, D., Schindler, K., Koltun, V.: Towards robust monocular depth estimation: Mixing datasets for zero-shot cross-dataset transfer. IEEE Transactions on Pattern Analysis and Machine Intelligence **44**(3) (2022)
- [18] Yang, L., Kang, B., Huang, Z., Xu, X., Feng, J., Zhao, H.: Depth anything: Unleashing the power of large-scale unlabeled data. In: Proceedings of the IEEE/CVF Conference on Computer Vision and Pattern Recognition (2024)
- [19] Yin, W., Zhang, C., Chen, H., Cai, Z., Yu, G., Wang, K., Chen, X., Shen, C.: Metric3d: Towards zero-shot metric 3d prediction from a single image. In: Proceedings of the IEEE/CVF International Conference on Computer Vision (2023)
- [20] Miangoleh, S.M.H., Dille, S., Mai, L., Paris, S., Aksoy, Y.: Boosting monocular depth estimation models to high-resolution via content-adaptive multi-resolution merging. In: Proceedings of the IEEE/CVF Conference on Computer Vision and Pattern Recognition, pp. 9685–9694 (2021)
- [21] Song, J., Park, S., An, H., Cho, S., Kwak, M.-S., Cho, S., Kim, S.: Därf: boosting radiance fields from sparse inputs with monocular depth adaptation. In: Advances in Neural Information Processing Systems, pp. 68458–68470 (2023)
- [22] Zhang, C., Yin, W., Wang, B., Yu, G., Fu, B., Shen, C.: Hierarchical normalization for robust monocular depth estimation. Advances in Neural Information Processing Systems **35**, 14128–14139 (2022)
- [23] Eigen, D., Puhrsch, C., Fergus, R.: Depth map prediction from a single image using a multi-scale deep network. In: Advances in Neural Information Processing Systems, pp. 2366–2374 (2014)
- [24] Sajjan, S.S., Moore, M.J., Pan, M., Nagaraja, G., Lee, J., Zeng, A., Song, S.: Clear grasp: 3d shape estimation of transparent objects for manipulation. IEEE International Conference on Robotics and Automation, 3634–3642 (2019)
- [25] Zimmermann, C., Brox, T.: Learning to estimate 3d hand pose from single rgb images. In: Proceedings of the IEEE/CVF International Conference on Computer Vision (2017)
- [26] Eigen, D., Fergus, R.: Predicting depth, surface normals and semantic labels with a common multi-scale convolutional architecture. In: Proceedings of the IEEE/CVF International Conference on Computer Vision, pp. 2650–2658 (2015)
- [27] Liu, F., Shen, C., Lin, G.: Deep convolutional

- neural fields for depth estimation from a single image. In: Proceedings of the IEEE/CVF Conference on Computer Vision and Pattern Recognition, pp. 5162–5170 (2015)
- [28] Yuan, W., Gu, X., Dai, Z., Zhu, S., Tan, P.: Newcrfs: Neural window fully-connected crfs for monocular depth estimation. In: Proceedings of the IEEE/CVF Conference on Computer Vision and Pattern Recognition (2022)
- [29] Shao, S., Pei, Z., Wu, X., Liu, Z., Chen, W., Li, Z.: Iebins: Iterative elastic bins for monocular depth estimation. In: Advances in Neural Information Processing Systems (2023)
- [30] Roy, A., Todorovic, S.: Monocular depth estimation using neural regression forest. In: Proceedings of the IEEE/CVF Conference on Computer Vision and Pattern Recognition, pp. 5506–5514 (2016)
- [31] Cheng, Z., Zhang, Y., Tang, C.: Swin-depth: Using transformers and multi-scale fusion for monocular-based depth estimation. IEEE Sensors Journal **21**(23), 26912–26920 (2021) <https://doi.org/10.1109/JSEN.2021.3120753>
- [32] Ke, B., Obukhov, A., Huang, S., Metzger, N., Daudt, R.C., Schindler, K.: Repurposing diffusion-based image generators for monocular depth estimation. In: Proceedings of the IEEE/CVF Conference on Computer Vision and Pattern Recognition, pp. 9492–9502 (2024)
- [33] Garg, R., Kumar, B.V., Carneiro, G., Reid, I.: Unsupervised cnn for single view depth estimation: Geometry to the rescue. In: Proceedings of the European Conference on Computer Vision, pp. 740–756 (2016). Springer
- [34] Godard, C., Mac Aodha, O., Brostow, G.J.: Unsupervised monocular depth estimation with left-right consistency. In: Proceedings of the IEEE/CVF Conference on Computer Vision and Pattern Recognition (2017)
- [35] Hu, M., Yin, W., Zhang, C., Cai, Z., Long, X., Chen, H., Wang, K., Yu, G., Shen, C., Shen, S.: Metric3d v2: A versatile monocular geometric foundation model for zero-shot metric depth and surface normal estimation. arXiv preprint arXiv:2404.15506 (2024)
- [36] Piccinelli, L., Yang, Y.-H., Sakaridis, C., Segu, M., Li, S., Van Gool, L., Yu, F.: UniDepth: Universal monocular metric depth estimation. In: Proceedings of the IEEE/CVF Conference on Computer Vision and Pattern Recognition (2024)
- [37] Yang, L., Kang, B., Huang, Z., Zhao, Z., Xu, X., Feng, J., Zhao, H.: Depth anything v2. arXiv:2406.09414 (2024)
- [38] Nazir, D., Pagani, A., Liwicki, M., Stricker, D., Afzal, M.Z.: Semattnet: Towards attention-based semantic aware guided depth completion. IEEE Access, 1–1 (2022) <https://doi.org/10.1109/ACCESS.2022.3214316>
- [39] Zhang, C., Tang, Y., Zhao, C., Sun, Q., Ye, Z., Kurths, J.: Multitask gans for semantic segmentation and depth completion with cycle consistency. IEEE Transactions on Neural Networks and Learning Systems **32**, 5404–5415 (2020)
- [40] Gu, J., Xiang, Z., Yuwen, Y., Wang, L.: Denselidar: A real-time pseudo dense depth guided depth completion network. IEEE Robotics and Automation Letters, 1–1 (2021) <https://doi.org/10.1109/LRA.2021.3060396>
- [41] Lee, S., Lee, J., Kim, D., Kim, J.: Deep architecture with cross guidance between single image and sparse lidar data for depth completion. IEEE Access **8**, 79801–79810 (2020) <https://doi.org/10.1109/ACCESS.2020.2990212>
- [42] Li, A., Yuan, Z., Ling, Y., Chi, W., Zhang, C., et al.: A multi-scale guided cascade hourglass network for depth completion. In: The IEEE Winter Conference on Applications of Computer Vision, pp. 32–40 (2020)
- [43] Xu, Y., Zhu, X., Shi, J., Zhang, G., Bao, H., Li, H.: Depth completion from sparse lidar data with depth-normal constraints. In: Proceedings of the IEEE/CVF International Conference on Computer Vision, pp. 2811–2820 (2019). <https://doi.org/10.1109/ICCV.2019.00290>
- [44] Yang, Y., Wong, A., Soatto, S.: Dense depth posterior (ddp) from single image and sparse range. In: Proceedings of the IEEE/CVF Conference on Computer Vision and Pattern Recognition, pp. 3348–3357 (2019). <https://api.semanticscholar.org/CorpusID:59336296>
- [45] Zhao, S., Gong, M., Fu, H., Tao, D.: Adaptive context-aware multi-modal network for depth completion. IEEE Transactions on Image

- Processing (2021)
- [46] Cheng, X., Wang, P., Guan, C., Yang, R.: Cspn++: Learning context and resource aware convolutional spatial propagation networks for depth completion. In: Proceedings of the AAAI Conference on Artificial Intelligence, pp. 10615–10622 (2020). <https://doi.org/10.1609/aaai.v34i07.6635>
- [47] Park, J.-H., Jeong, C., Lee, J., Jeon, H.-G.: Depth prompting for sensor-agnostic depth estimation. In: Proceedings of the IEEE/CVF Conference on Computer Vision and Pattern Recognition, pp. 9859–9869 (2024)
- [48] Liu, T.Y., Agrawal, P., Chen, A., Hong, B.-W., Wong, A.: Monitored distillation for positive congruent depth completion. In: Avidan, S., Brostow, G., Cissé, M., Farinella, G.M., Hassner, T. (eds.) Proceedings of the European Conference on Computer Vision, pp. 35–53 (2022)
- [49] Lopez-Rodriguez, A., Busam, B., Mikolajczyk, K.: Project to adapt: Domain adaptation for depth completion from noisy and sparse sensor data. In: Asian Conference on Computer Vision (2020)
- [50] Wong, A., Soatto, S.: Unsupervised depth completion with calibrated backprojection layers. In: Proceedings of the IEEE/CVF International Conference on Computer Vision, pp. 12747–12756 (2021)
- [51] Wong, A., Fei, X., Tsuei, S., Soatto, S.: Unsupervised depth completion from visual inertial odometry. *IEEE Robotics and Automation Letters* **5**(2), 1899–1906 (2020)
- [52] Wong, A., Cicek, S., Soatto, S.: Learning topology from synthetic data for unsupervised depth completion. *IEEE Robotics and Automation Letters* **6**(2), 1495–1502 (2021)
- [53] Wong, A., Fei, X., Hong, B.-W., Soatto, S.: An adaptive framework for learning unsupervised depth completion. *IEEE Robotics and Automation Letters* **6**(2), 3120–3127 (2021)
- [54] Chawla, J., Thakurdesai, N., Godase, A., Reza, M., Crandall, D., Jung, S.-H.: Error diagnosis of deep monocular depth estimation models. In: Proceedings of the IEEE/RSJ International Conference on Intelligent Robots and Systems (IROS), pp. 5344–5649 (2021). IEEE
- [55] Mustafa, A., Mikhailiuk, A., Iliescu, D.A., Babbar, V., Mantiuk, R.K.: Training a task-specific image reconstruction loss. In: Proceedings of the IEEE/CVF Winter Conference on Applications of Computer Vision, pp. 2319–2328 (2022)
- [56] Zhao, H., Gallo, O., Frosio, I., Kautz, J.: Loss functions for image restoration with neural networks. *IEEE Transactions on computational imaging* **3**(1), 47–57 (2016)
- [57] Silberman, N., Hoiem, D., Kohli, P., Fergus, R.: Indoor segmentation and support inference from rgbd images. In: Proceedings of the European Conference on Computer Vision, pp. 746–760 (2012). Springer
- [58] Uhrig, J., Schneider, N., Schneider, L., Franke, U., Brox, T., Geiger, A.: Sparsity invariant cnns. In: International Conference on 3D Vision (2017). IEEE
- [59] Kirillov, A., Mintun, E., Ravi, N., Mao, H., Rolland, C., Gustafson, L., Xiao, T., Whitehead, S., Berg, A.C., Lo, W.-Y., Dollar, P., Girshick, R.: Segment anything. In: Proceedings of the IEEE/CVF International Conference on Computer Vision, pp. 4015–4026 (2023)
- [60] Kingma, D.P., Ba, J.: Adam: A method for stochastic optimization. In: ICLR (2015)
- [61] Paszke, A., Gross, S., Massa, F., Lerer, A., Bradbury, J., Chanan, G., Killeen, T., Lin, Z., Gimelshein, N., Antiga, L., et al.: PyTorch: An imperative style, high-performance deep learning library. *Advances in Neural Information Processing Systems* (2019)
- [62] Alhashim, B., Wonka, P.: High quality monocular depth estimation via transfer learning. *arXiv preprint arXiv:1812.11941* (2018) [arXiv:1812.11941 \[cs.CV\]](https://arxiv.org/abs/1812.11941)
- [63] Zhang, Y., Funkhouser, T.: Deep depth completion of a single rgbd image. In: Proceedings of the IEEE/CVF Conference on Computer Vision and Pattern Recognition (2018)
- [64] Zhu, L., Mousavian, A., Xiang, Y., Mazhar, H., Eenbergen, J., Debnath, S., Fox, D.: Rgb-d local implicit function for depth completion of transparent objects. In: Proceedings of the IEEE/CVF Conference on Computer Vision and Pattern Recognition (2021)
- [65] Xu, H., Wang, Y.R., Eppel, S., Aspuru-Guzik, A., Shkurti, F., Garg, A.: Seeing

glass: Joint point cloud and depth completion for transparent objects. In: Conference on Robot Learning (CoRL) (2021). <https://arxiv.org/abs/2110.00087>